

# Characteristics of hybrid compact stars with a sharp hadron-quark interface

Mark G. Alford and Sophia Han <sup>a</sup>

Physics Department, Washington University, St. Louis, Missouri 63130, USA

Received: date / Revised version: date

**Abstract.** We describe two aspects of the physics of hybrid stars that have a sharp interface between a core of quark matter and a mantle of nuclear matter. Firstly, we analyze the mass-radius relation. We describe a generic “Constant Speed of Sound” (CSS) parameterization of the quark matter equation of state (EoS), in which the speed of sound is independent of density. In terms of the three parameters of the CSS EoS we obtain the phase diagram of possible forms of the hybrid star mass-radius relation, and we show how observational constraints on the maximum mass and typical radius of neutron stars can be expressed as constraints on the CSS parameters. Secondly, we propose a mechanism for the damping of density oscillations, including r-modes, in hybrid stars with a sharp interface. The dissipation arises from the periodic conversion between quark matter and nuclear matter induced by the pressure oscillations in the star. We find the damping grows nonlinearly with the amplitude of the oscillation and is powerful enough to saturate an r-mode at very low saturation amplitude, of order  $10^{-10}$ , which is compatible with currently-available observations of neutron star spin frequencies and temperatures.

**PACS.** 25.75.Nq Quark deconfinement, quark-gluon plasma production, and phase transitions – 26.60.-c Nuclear matter aspects of neutron stars – 97.60.Jd Neutron stars

## 1 Introduction

One of the major goals of nuclear physics is to establish the nature and properties of matter at nuclear density and beyond. Experimental constraints on the properties of ultra-high-density matter come from neutron stars, where gravity compresses matter to the highest densities found in nature. One hypothesis is that there is a phase transition from nuclear matter to quark matter, and that some stars, called “hybrid stars”, contain cores of quark matter.

We will assume that in hybrid stars the core of quark matter and the mantle of nuclear matter are separated by a sharp interface (Maxwell construction) as opposed to a mixed phase (Gibbs construction). This assumption is valid if the nuclear-quark phase transition is first order, and the surface tension of the interface is high enough. This is a possible scenario, given the uncertainties in the value of the surface tension [1–3]. For analysis of generic equations of state that continuously interpolate between the phases to model mixing or percolation, see Refs. [4, 5].

In this paper we discuss two aspects of the physics of such hybrid stars, each of which is relevant to a different set of observable properties of the star.

Firstly, in Secs. 2 to 4, we analyze the mass-radius relation of hybrid stars, using a generic parameterization of the quark matter equation of state (EoS). We obtain the phase diagram of possible forms of the hybrid star mass-radius relation, and we

show how observational constraints on the maximum mass and typical radius of hybrid stars can be expressed as constraints on the parameters of the quark matter EoS.

Secondly, in Sec. 5, we propose a mechanism for the damping of density oscillations in hybrid stars with a sharp interface. Such damping is important for the occurrence and saturation of r-modes [6, 7], which if undamped can spin down a star in days via emission of gravitational radiation. The relevant observables in this case are the spin frequency, spindown rate, and temperature of the star. Our proposed damping mechanism arises from the periodic conversion between quark matter and nuclear matter induced by the pressure oscillations in the star. We find the damping grows nonlinearly with the amplitude of the oscillation and is powerful enough to saturate an r-mode at very low saturation amplitude, of order  $10^{-10}$ , which is compatible with currently-available observations of neutron star spin frequencies and temperatures.

## 2 The CSS parameterization

The equation of state (EoS) of quark matter at the densities and temperatures relevant to neutron stars has not yet been calculated from first principles. There are many models available, each based on some simplification of the real physics, and each with their own parameters. It is therefore useful to have a general parameterization of the EoS which can be used as a generic language for relating different models to each other and for expressing experimental constraints in model-independent terms.

<sup>a</sup> e-mail: jhan@physics.wustl.edu

We will use the “Constant Speed of Sound” (CSS) parameterization [8–10], which can be viewed as the lowest-order terms of a Taylor expansion of the quark matter EoS about the transition pressure  $p_{\text{trans}}$ . As illustrated in Fig. 1, one can then write the high-density EoS in terms of three parameters: the pressure  $p_{\text{trans}}$  of the transition, the discontinuity in energy density  $\Delta\epsilon$  at the transition, and the speed of sound  $c_{\text{QM}}$  in the high-density phase. For a given nuclear matter EoS  $\epsilon_{\text{NM}}(p)$ , the full CSS EoS is then

$$\epsilon(p) = \begin{cases} \epsilon_{\text{NM}}(p) & p < p_{\text{trans}} \\ \epsilon_{\text{NM}}(p_{\text{trans}}) + \Delta\epsilon + c_{\text{QM}}^2(p - p_{\text{trans}}) & p > p_{\text{trans}} \end{cases}, \quad (1)$$

where  $\epsilon_{\text{NM}}(p)$  is the nuclear matter equation of state.

The assumption of a density-independent speed of sound is accurate for a large class of models of quark matter, including many Nambu–Jona-Lasinio models [9, 11–13], the perturbative quark matter EoS [14], and the quartic polynomial parameterization [15]. For details, see Ref. [16]. It is noticeable that models based on relativistic quarks tend to have  $c_{\text{QM}}^2 \approx$  close to  $1/3$ , which is the value for systems with conformal symmetry, and it has been conjectured that there is a fundamental bound  $c_{\text{QM}}^2 < 1/3$  [17], although some models violate that bound, e.g. [18, 19] or [13] (parameterized in [9]).

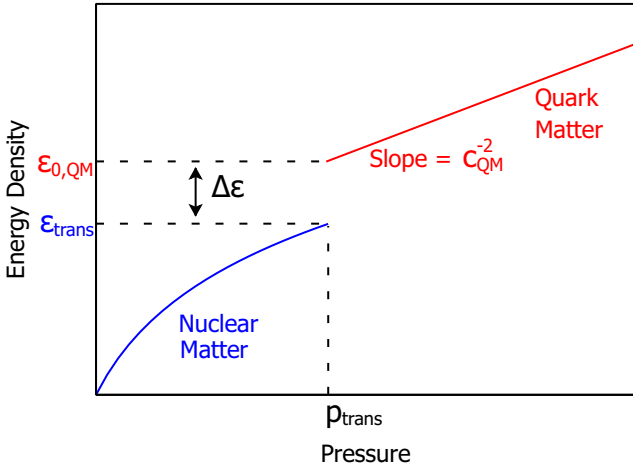


**Fig. 1.** Equation of state  $\epsilon(p)$  for dense matter. The quark matter EoS is specified by the transition pressure  $p_{\text{trans}}$ , the energy density discontinuity  $\Delta\epsilon$ , and the speed of sound in quark matter  $c_{\text{QM}}$  (assumed density-independent).

At pressures below  $p_{\text{trans}}$  we use two examples of nuclear EoS: Dirac-Brueckner-Hartree-Fock (DBHF) [22] and Brueckner-Hartree-Fock (BHF) [23]. Some of the properties of BHF and DBHF are summarized in Table 1, where  $L$  is related to the derivative of the symmetry energy  $S_0$  with respect to density at the nuclear saturation density,  $L = 3n_0(\partial S_0/\partial n)|_{n_0}$ . BHF is a softer equation of state, with a lower value of  $L$  and lower pressure at a given energy density. DBHF is a stiffer EoS, with higher pressure at a given energy density. It yields neutron stars that are larger, and can reach a higher maximum mass. With CSS parametrization for quark matter and realistic nuclear matter EoSes, we study in detail what possible forms of hybrid star

property	BHF, Av18 + UVIX TBF	DBHF, Bonn A
saturation baryon density $n_0(\text{fm}^{-3})$	0.16	0.18
binding energy/baryon $E/A$ (MeV)	-15.98	-16.15
compressibility $K_0$ (MeV)	212.4	230
symmetry energy $S_0$ (MeV)	31.9	34.4
$L = 3n_0(\partial S_0/\partial n) _{n_0}$ (MeV)	52.9	69.4
maximum mass of star ( $M_\odot$ )	2.03	2.31
radius of the heaviest star (km)	9.92	11.26
radius of $M = 1.4 M_\odot$ star (km)	11.77	13.41

**Table 1.** Calculated properties of symmetric nuclear matter for the BHF and DBHF nuclear equations of state used here. BHF is softer, DBHF is stiffer.

mass-radius relations are and how they rely on the high-density phase parameter values.

In Sec. 3 we show how the CSS parameterization is constrained by observables such as the maximum mass  $M_{\text{max}}$ , the radius of a maximum-mass star, and the radius  $R_{1.4}$  of a star of mass  $1.4 M_\odot$ , based on BHF and DBHF nuclear matter EoSes.

### 3 Generic conditions for stable hybrid stars

A compact star will be stable as long as the mass  $M$  of the star is an increasing function of the central pressure  $p_{\text{cent}}$  [24]. By performing an expansion in powers of the size of the quark matter core, it has been shown [25, 20, 21] that the appearance of a quark matter core when  $p_{\text{cent}}$  rises above  $p_{\text{trans}}$  will only destabilize the star if the energy density discontinuity  $\Delta\epsilon$  is too large, specifically if  $\Delta\epsilon > \Delta\epsilon_{\text{crit}}$  where

$$\frac{\Delta\epsilon_{\text{crit}}}{\epsilon_{\text{trans}}} = \frac{1}{2} + \frac{3}{2} \frac{p_{\text{trans}}}{\epsilon_{\text{trans}}}. \quad (2)$$

(This is  $\lambda_{\text{crit}} - 1$  in the notation of Ref. [20].)

In Fig. 2, panels (b) and (c) show possible forms of  $M(R)$  for  $\Delta\epsilon < \Delta\epsilon_{\text{crit}}$ , where a stable connected hybrid branch continues on from the hadronic branch of the  $M(R)$  relation. Panels (a) and (d) show possible forms for  $\Delta\epsilon > \Delta\epsilon_{\text{crit}}$ , where there is no stable connected branch, although in (d) there is a disconnected one. In Figs. 2 (b) and (d), we illustrate how, as noted in Ref. [20], a second, disconnected, branch of stable hybrid stars can arise. The disconnected branch is a “third family” [26, 27] of compact stars besides neutron stars and white dwarfs. In  $M(R)$  curves for realistic neutron star equations of state, The cusp that occurs where an unstable hybrid branch meets the hadronic branch is exaggerated in Fig. 2. In  $M(R)$  plots for realistic EoSes the cusp is invisibly small, covering a range in  $M$  of less than one part in a thousand.

#### 3.1 Phase diagram at fixed $c_{\text{QM}}$

In Fig. 3 we plot a “phase diagram” for hybrid stars showing how the form of the  $M(R)$  relation depends on the CSS parameters  $p_{\text{trans}}/\epsilon_{\text{trans}}$  and  $\Delta\epsilon/\epsilon_{\text{trans}}$  at fixed  $c_{\text{QM}}^2$  (see Ref. [8, 16]). The left panel of Fig. 3 is the result of calculations for the BHF

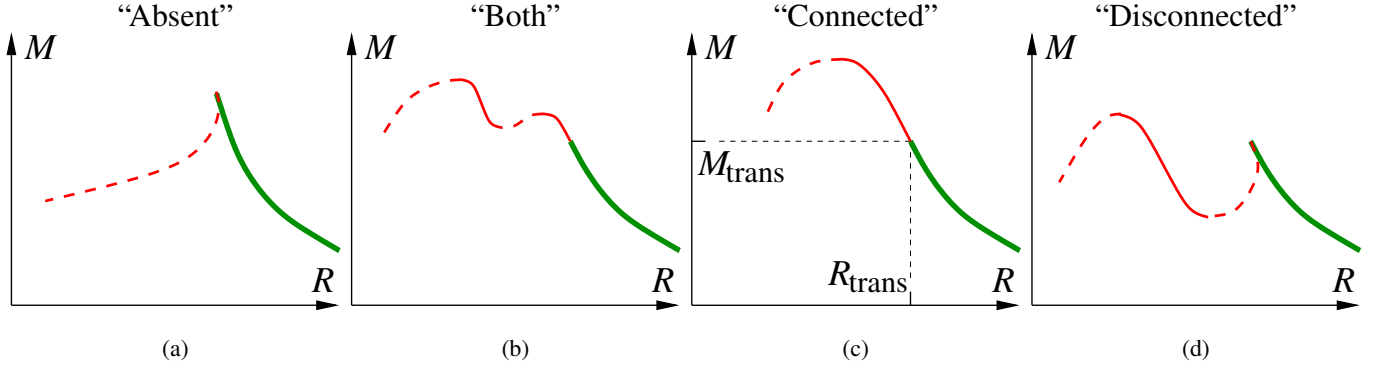


**Fig. 2.** (Color online) Schematic form of possible mass-radius relations for hybrid stars. The thick (green) line is the hadronic branch. Thin solid (red) lines are stable hybrid stars; thin dashed (red) lines are unstable hybrid stars. In (a) the hybrid branch is absent. In (c) there is a connected branch. In (d) there is a disconnected branch. In (b) there are both types of branch. In realistic neutron star  $M(R)$  curves the cusp that occurs in cases (a) and (d) is much smaller and harder to see [20, 21].

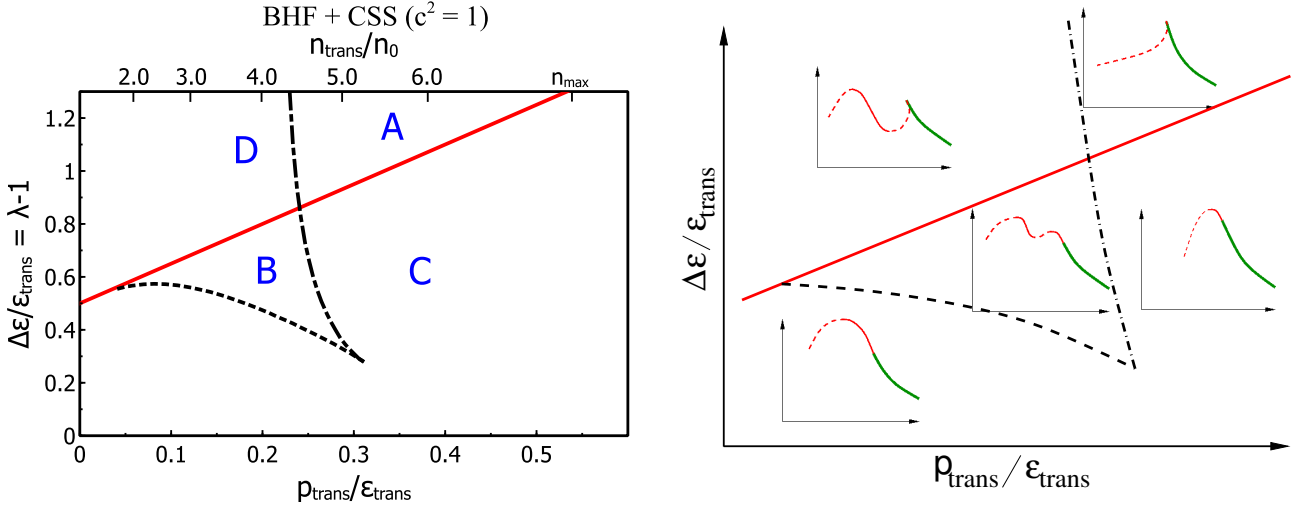


**Fig. 3.** (Color online) Phase diagram for hybrid star branches in the mass-radius relation of compact stars.

nuclear matter EoS and quark matter with  $c_{QM}^2 = 1$ . The right panel is a schematic showing the form of the mass-radius relation in each region of the diagram. The regions correspond to different geometries of the hybrid branch displayed in Fig. 2: A=“Absent”, C=“Connected”, D=“Disconnected”, B=“Both” (connected and disconnected).

The solid straight (red) line is  $\Delta\epsilon_{\text{crit}}$  from Eq. (2). Below the line in regions B and C, there is a hybrid star branch connected to the nuclear star branch. Above the line in regions A and D, there is no connected hybrid star branch. In regions B and D there is a disconnected hybrid star branch.

The roughly vertical dash-dotted curve in Fig. 3 marks a transition where a the disconnected branch of hybrid stars appears/disappears. When one crosses this line from the right, going from region A to D by decreasing the nuclear/quark transition density, a stationary point of inflection appears in  $M(p_{\text{cent}})$  at  $p_{\text{cent}} > p_{\text{trans}}$ . If one crosses from C to B then this point of inflection is at lower central pressure than the existing maximum in  $M(p_{\text{cent}})$ . This produces a stationary point of inflection

in the  $M(R)$  relation to the left of the existing maximum (if any). After crossing the dash-dotted line the point of inflection becomes a new maximum-minimum pair (the maximum being further from the transition point), producing a disconnected branch of stable hybrid stars in regions B and D. Crossing the other way, by increasing the transition pressure, the maximum and minimum that delimit the disconnected branch merge and the branch disappears.

The roughly horizontal dashed curve in Fig. 3 which separates region B and C marks a transition between mass-radius relations with one connected hybrid star branch, and those with two hybrid star branches, one connected and one disconnected. Crossing this line from below, by increasing the energy density discontinuity, a stationary point of inflection in  $M(p_{\text{cent}})$  (or equivalently in  $M(R)$ ) appears in the existing connected hybrid branch. Crossing in to region B, this point of inflection becomes a new maximum-minimum pair, so the connected hybrid branch is broken in to a smaller connected branch and a new disconnected branch. The maximum of the old connected

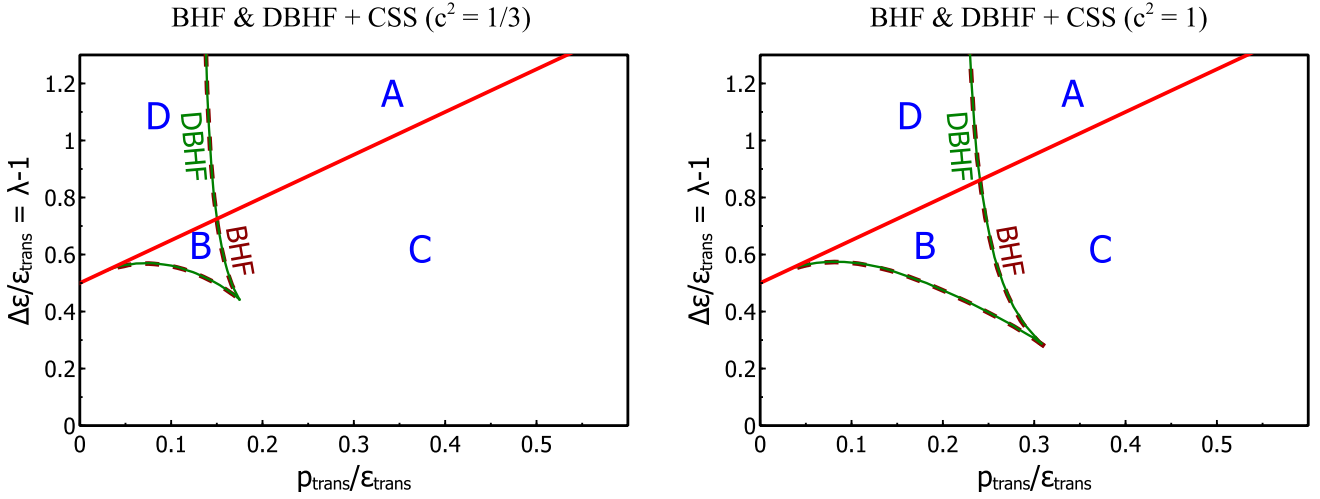


**Fig. 4.** (Color online) Phase diagram like Fig. 3, showing that the phase boundaries are very insensitive to changes in the nuclear matter EoS, but they are affected by varying the quark matter speed of sound. Note that, for a given pressure, BHF and DBHF have very different baryon densities.

branch smoothly becomes the maximum of the new disconnected branch. If one crossed the dashed line in the opposite direction, from B to C, the maximum closest to the transition point would approach the minimum and they would annihilate, leaving only the more distant maximum.

Where the horizontal and vertical curves meet, the two maxima and the minimum that are present in region B all merge to form a single flat maximum where the first three derivatives of  $M(R)$  are all zero.

### 3.2 Varying $c_{\text{QM}}^2$ and the nuclear EoS

In Fig. 4 we show the effects of varying the speed of sound and the nuclear matter EoS. Fig. 4(a) is the phase diagram with  $c_{\text{QM}}^2 = 1/3$  (characteristic of very weakly interacting massless quarks), and Fig. 4(b) is for  $c_{\text{QM}}^2 = 1$  (the maximum value consistent with causality). In both panels we show the phase diagram for BHF and DBHF nuclear matter EoS. The straight line is independent of  $c_{\text{QM}}^2$  and the detailed form of the nuclear matter EoS. The other phase boundaries, outlining the region where there is a disconnected hybrid branch, are remarkably insensitive to the details of the nuclear matter EoS but depend strongly on the quark matter speed of sound. For a given nuclear matter EoS the hybrid branch structure is determined by  $p_{\text{trans}}/\epsilon_{\text{trans}}$ ,  $\Delta\epsilon/\epsilon_{\text{trans}}$ , and  $c_{\text{QM}}^2$ , so one could make a three-dimensional plot with  $c_{\text{QM}}^2$  as the third axis, but this figure adequately illustrates the dependence on  $c_{\text{QM}}^2$ . We will now discuss the physics behind the shape of the phase boundaries.

### 3.3 Physical understanding of the phase diagram

The main feature of the phase diagram is that a disconnected branch is present when the transition density is sufficiently low,

and the energy density discontinuity is sufficiently high. It occurs more readily if the speed of sound in quark matter is high.

When a very small quark matter core is present, its greater density creates an additional gravitational pull on the nuclear mantle. If the pressure of the core can counteract the extra pull, the star is stable and there is a connected hybrid branch. If the energy density jump is too great, the extra gravitational pull is too strong, and the star becomes unstable when quark matter first appears. However, if the energy density of the core rises slowly enough with increasing pressure (i.e. if  $c^2 = dp/d\epsilon$  is large enough), a larger core with a higher central pressure may be able to sustain the weight of the nuclear mantle above it. Region B, with connected and disconnected branches, is more complicated and we do not have an intuitive explanation for it.

We can now understand why the vertical line marking the B/C and D/A boundaries moves to the right as  $c_{\text{QM}}^2$  increases. Since  $c^2 = dp/d\epsilon$ , if  $c_{\text{QM}}^2$  is larger then the energy density of the core rises more slowly with increasing pressure, which minimizes the tendency for a large core to destabilize the star via its gravitational attraction. Finally, we can see why that line has a slight negative slope: larger  $\Delta\epsilon$  makes the quark core heavier, increasing its pull on the nuclear mantle, and making the hybrid star more unstable against collapse.

## 4 Constraining a generic high-density equation of state

### 4.1 Maximum mass of hybrid stars

In Fig. 5 [16] we show how mass measurements of neutron stars can be expressed as constraints on the CSS parameters; the upper plots are for DBHF and the lower plots are for BHF nuclear matter EoS. Each panel shows dependence on  $p_{\text{trans}}/\epsilon_{\text{trans}}$  and  $\Delta\epsilon/\epsilon_{\text{trans}}$  for fixed  $c_{\text{QM}}^2$ . The region in which the transition to quark matter would occur below nuclear saturation density

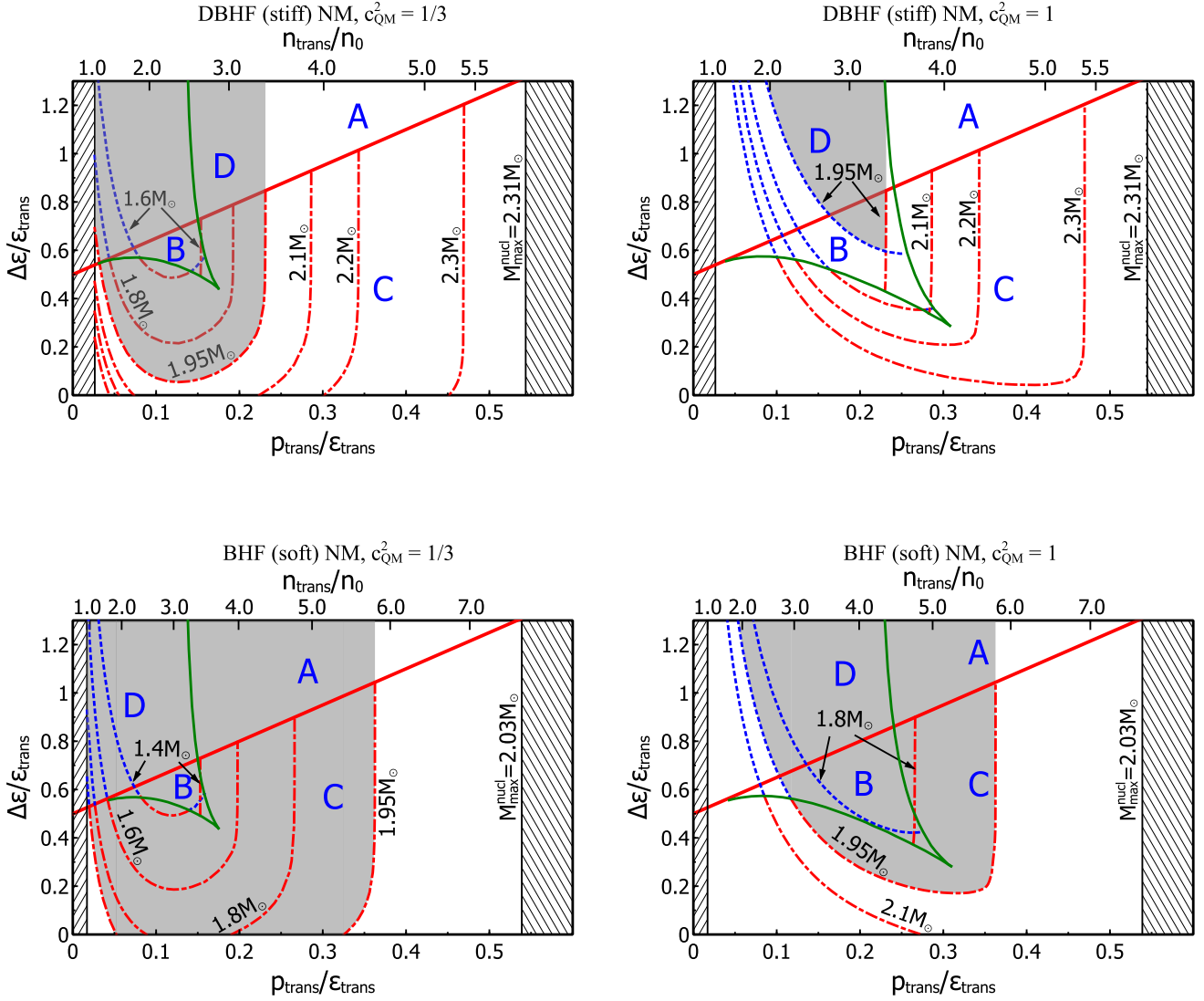


**Fig. 5.** (Color online) Contour plots showing the maximum hybrid star mass as a function of the CSS parameters of the high-density EoS. Each panel shows the dependence on the CSS parameters  $p_{\text{trans}}/\epsilon_{\text{trans}}$  and  $\Delta\epsilon/\epsilon_{\text{trans}}$ . The left plots are for  $c_{\text{QM}}^2 = 1/3$ , and the right plots are for  $c_{\text{QM}}^2 = 1$ . The top row is for a DBHF (stiff) nuclear matter EoS, and the bottom row is for a BHF (soft) nuclear matter EoS. The grey shaded region, where  $M_{\text{max}} < 1.95M_{\odot}$ , is excluded by the observation of stars of mass  $M \approx 2M_{\odot}$ . The hatched band at low density (where  $n_{\text{trans}} < n_0$ ) is excluded because bulk nuclear matter would be metastable. The hatched band at high density is excluded because the transition pressure is above the central pressure of the heaviest stable hadronic star.

( $n_{\text{trans}} < n_0$ ) is excluded (hatched band at left end) because in that region bulk nuclear matter would be metastable. There is also an upper limit on the transition pressure, which is the central pressure of the heaviest stable nuclear matter star. This depends on the hadronic EoS that has been assumed.

The contours show the maximum mass of a hybrid star as a function of the EoS parameters. The grey shaded region, where  $M_{\text{max}} < 1.95M_{\odot}$ , contains quark matter EoSes that are excluded at the one to two  $\sigma$  level by the recent observations of stars of mass  $M \approx 2M_{\odot}$  [28] [29]. For high-density EoSes with  $c_{\text{QM}}^2 = 1$  (right hand plots), this region is not too large, and leaves a good range of transition pressures and energy density

discontinuities that are compatible with the observation. However, for high-density matter with  $c_{\text{QM}}^2 = 1/3$  (left hand plots), which is the typical value in many models (see Sec. 1), the  $M_{\text{max}} \gtrsim 2M_{\odot}$  constraint eliminates a large region of the CSS parameter space. As one would expect, the stiffer EoS gives rise to heavier (and larger) stars, and therefore allows a wider range of CSS parameters to be compatible with the  $2M_{\odot}$  measurement. The region B, where connected and disconnected hybrid star branches can coexist, is excluded for  $c_{\text{QM}}^2 \leq 1/3$ , and even for larger  $c_{\text{QM}}^2$  it is only allowed if the nuclear matter EoS is sufficiently stiff.

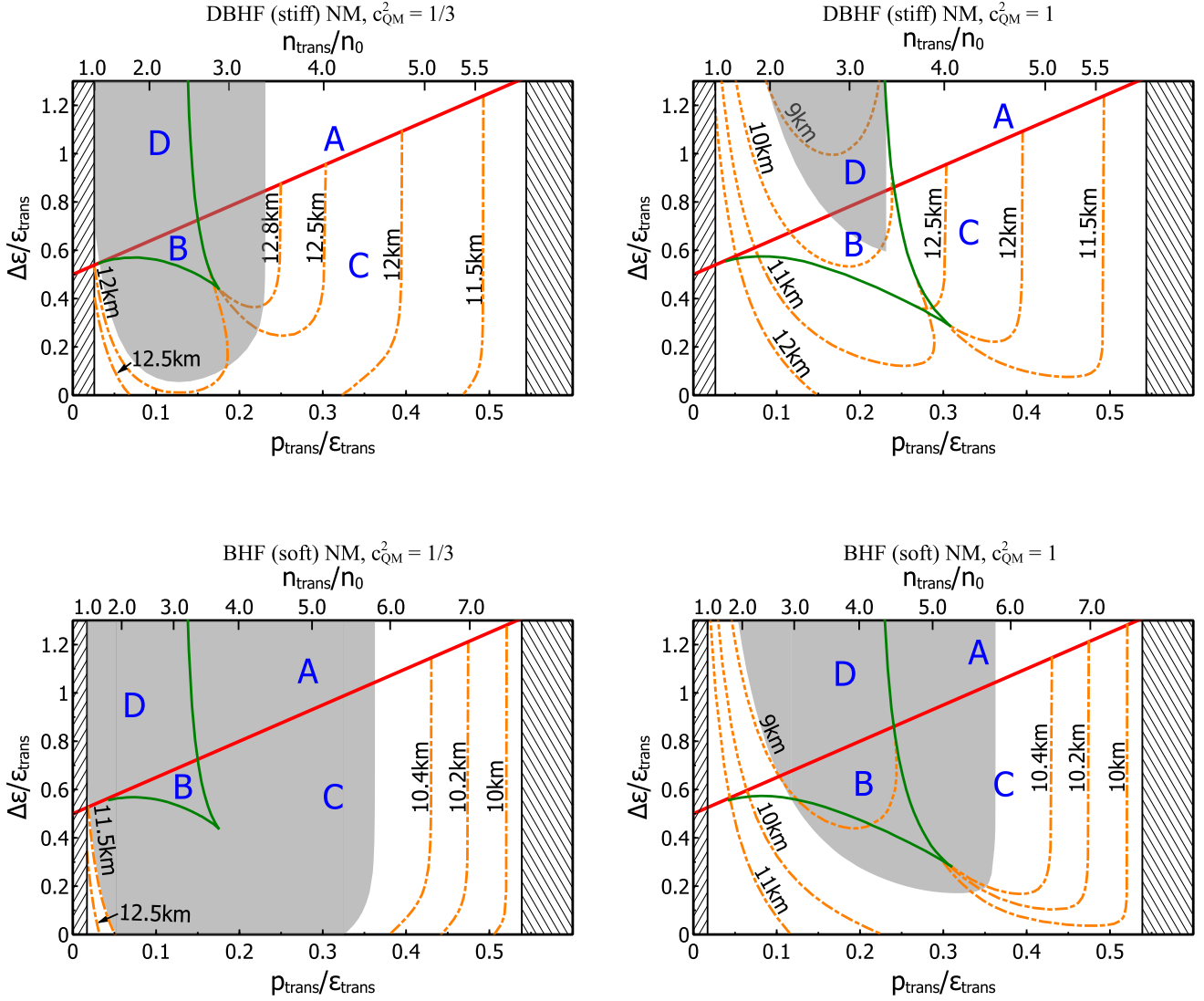


**Fig. 6.** (Color online) Contour plots showing the radius of the maximum-mass star as a function of the CSS parameters. Dashed lines are for the case where this star is on the disconnected branch; for dot-dashed lines it is on the connected branch. The grey shaded region where  $M_{\max} < 1.95 M_{\odot}$  is excluded by the measurement of a  $2M_{\odot}$  star. The hatched band at low density (where  $n_{\text{trans}} < n_0$ ) is excluded because bulk nuclear matter would be metastable. The hatched band at high density is excluded because the transition pressure is above the central pressure of the heaviest stable hadronic star. For a magnified version of the low-transition-pressure region for  $c_{\text{QM}}^2 = 1/3$ , see Fig. 8.

In Fig. 5 the dot-dashed (red) contours are for hybrid stars on a connected branch, while the dashed (blue) contours are for disconnected branches. When crossing the near-horizontal boundary from region C to B the maximum mass of the connected branch smoothly becomes the maximum mass of the disconnected branch, therefore the red contour in the C region smoothly becomes a blue contour in the B and D regions. When crossing the near-vertical boundary from region C to B a new disconnected branch forms, so the connected branch (red dot-dashed) contour crosses this boundary smoothly.

If, as predicted by many models,  $c_{\text{QM}}^2 \lesssim 1/3$ , then the existence of a  $2M_{\odot}$  star constrains the other CSS parameters to two regions of parameter space: in the left-hand region the

transition occurs at a fairly low density  $n_{\text{trans}} \lesssim 2n_0$ ; in the right-hand allowed region the transition pressure is high, and the connected branch contours are, except at very low  $\Delta\epsilon$ , almost vertical, corresponding to EoSes that give rise to a very small connected hybrid branch, and the maximum mass on this branch is very close to the mass of the purely-hadronic matter star with  $p_{\text{cent}} = p_{\text{trans}}$ . The mass of such a purely hadronic star is naturally independent of parameters that only affect the quark matter EoS, such as  $\Delta\epsilon$  and  $c_{\text{QM}}^2$ , so the contour is vertical. These hybrid stars have a tiny core of the high density phase and cover a tiny range of masses, of order  $10^{-3} M_{\odot}$  or less (see e.g., Fig. 5 in [8]), and so would be very rare.



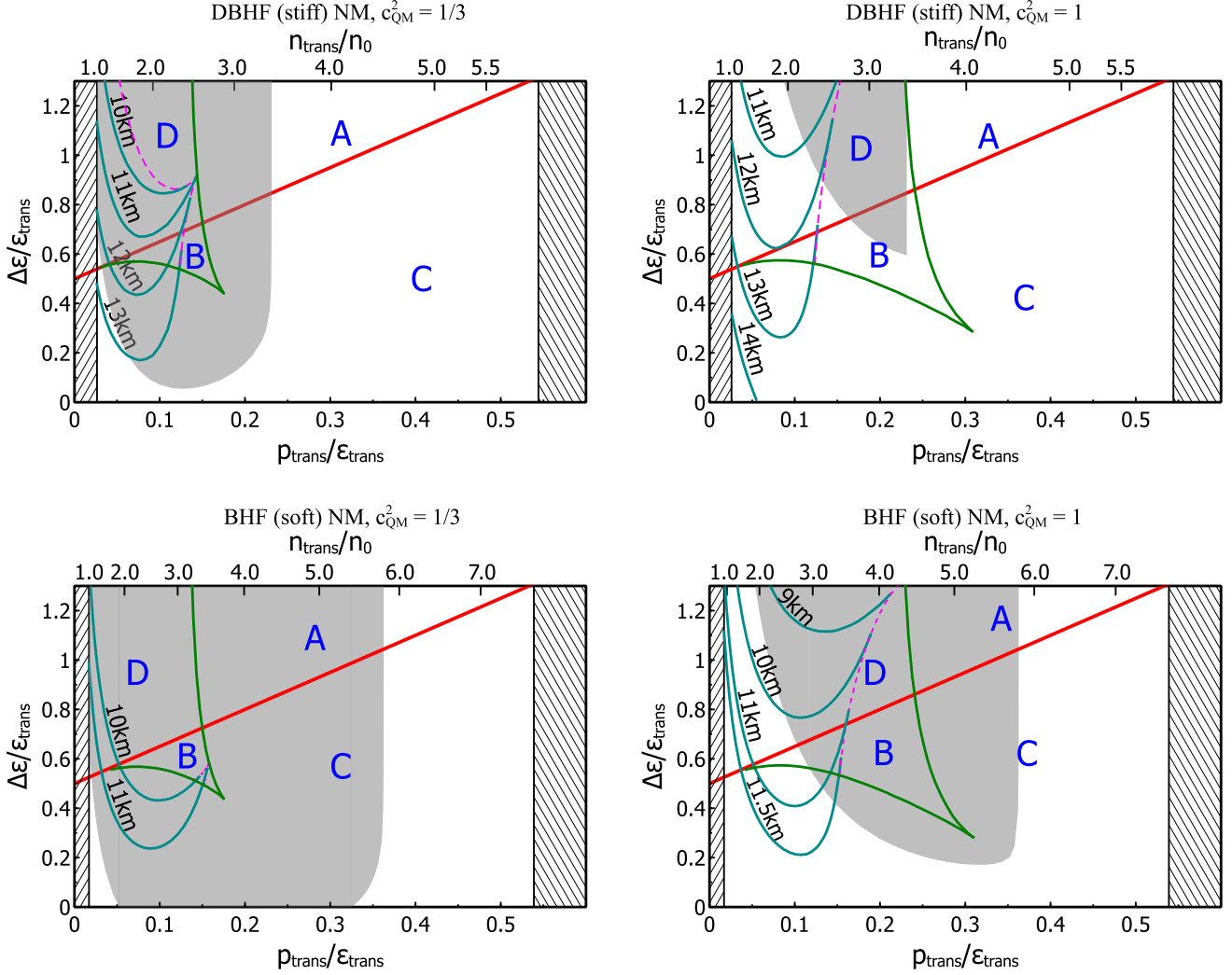


**Fig. 7.** (Color online) Contour plots similar to Fig. 6 showing the radius at a hybrid star of mass  $M = 1.4M_\odot$  as a function of the CSS parameters. Such stars only exist in a limited region of the space of EoSes (delimited by dashed (magenta) lines). Outside that region the only  $1.4M_\odot$  star is a hadronic star with radius 11.8 km (BHF) or 13.4 km (DBHF) (see Table 1). The grey shaded region where  $M_{\max} < 1.95M_\odot$  is excluded by the measurement of a  $2M_\odot$  star. For a magnified version of the low-transition-pressure region for  $c_{\text{QM}}^2 = 1/3$ , see Fig. 8.

## 4.2 Typical radius of hybrid stars

### 4.2.1 Minimum radius

In Fig. 6 we show contour plots of the radius of the maximum-mass star (on either a connected or disconnected hybrid branch) as a function of the CSS quark matter EoS parameters. Since the smallest hybrid star is typically the heaviest one, this allows us to infer the smallest radius that arises from a given EoS.

The smallest stars, with radii as small as 9 km, occur when the high-density phase has the largest possible speed of sound  $c_{\text{QM}}^2 = 1$ . They are disconnected branch stars arising from EoSes having a low transition pressure ( $n_{\text{trans}} \lesssim 2n_0$ ) with a fairly large energy density discontinuity ( $\Delta\epsilon/\epsilon_{\text{trans}} \gtrsim 1$ ). The contours in the high-transition-pressure region are almost vertical because the hybrid branch is a very short extension to the nuclear mass-radius relation, and its radius decreases with  $p_{\text{trans}}$  in this region, because it decreases with central pressure.

For  $c_{\text{QM}}^2 = 1/3$ , the allowed low-transition-pressure region is disconnected from the high-transition-pressure region and is so small that it is hard to see on this plot. By magnifying it (left panel of Fig. 8) we see that in this region the radius contours closely track the border of the allowed region (the  $M_{\max} = 1.95M_\odot$  line) so we can say that the radius must be greater than 11.25 km. For a stiff hadronic EoS this minimum is raised to 11.4 km. These values are comparable to the minimum radius of about 11.8 km found in Ref. [17], which explored a larger set of hadronic EoSes but did not explore the full CSS parameter space for the high-density EoS. If a star with radius smaller than this minimum value were to be observed, we would have to conclude that either the transition occurs outside the low-density region or that  $c_{\text{QM}}^2$  is greater than 1/3. In the magnified figure we also show how the excluded region would grow if a  $2.1M_\odot$  star were to be observed (long-dashed line for connected branch stars and short-dashed line for disconnected branch stars). This would increase the minimum radius

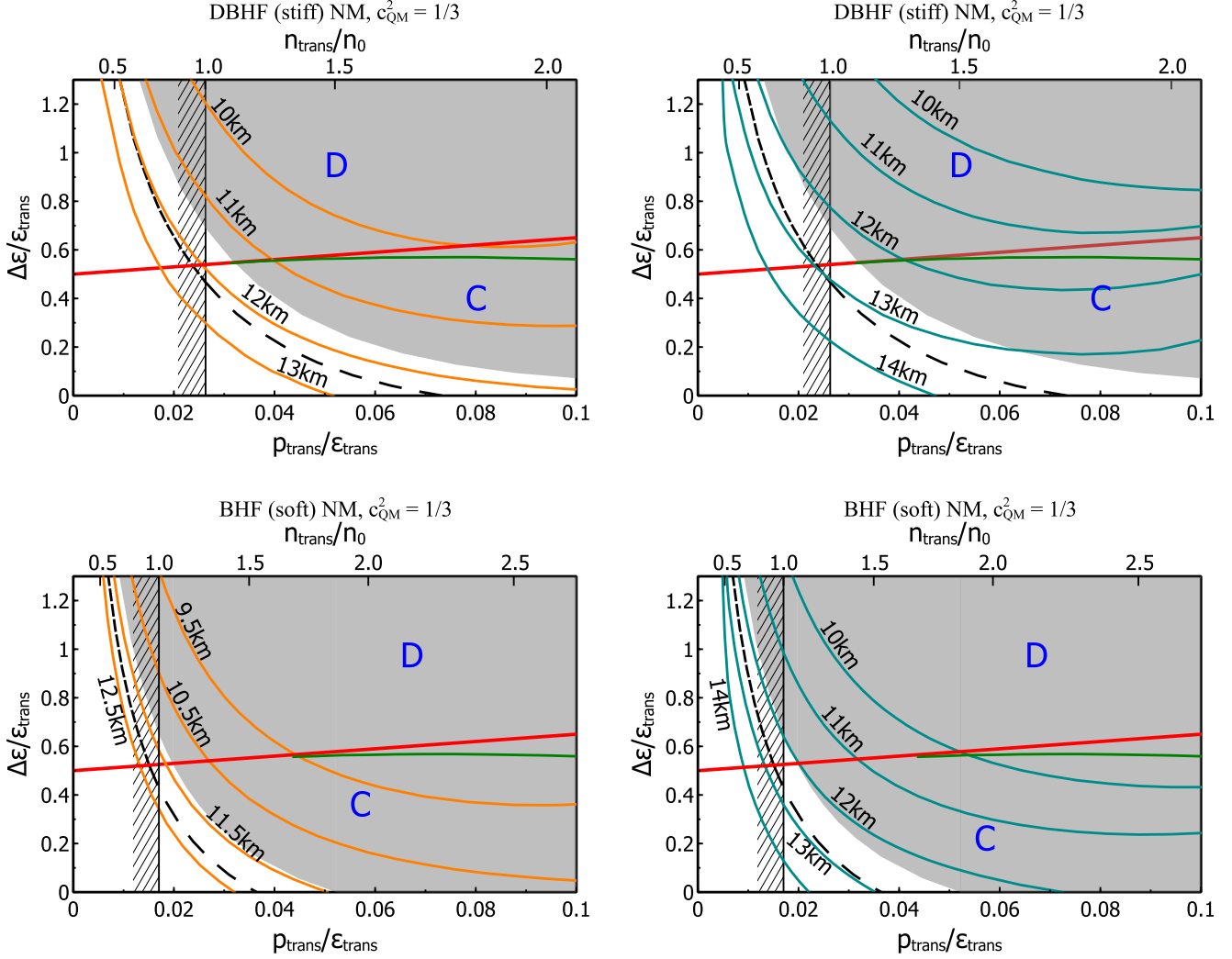


**Fig. 8.** (Color online) Magnified version of the  $c_{\text{QM}}^2 = 1/3$  plots in Figs. 6 and 7. In the two left panels, the contours are for the radius of the maximum mass star, which is typically the smallest star for the given EoS. In the two right panels, the contours are for  $R_{1.4}$ , the radius of a  $1.4 M_{\odot}$  star. The region under and to the left of the hatched bar is probably unphysical because  $n_{\text{trans}} < n_0$ , and it was excluded (hatched band) in earlier figures. The grey shaded region where  $M_{\text{max}} < 1.95 M_{\odot}$  is excluded by the measurement of a  $2 M_{\odot}$  star. The dashed line shows how that region would grow if a  $2.1 M_{\odot}$  star were observed.

to about 12.1 km for the soft hadronic EoS and 12.2 km for the stiff hadronic EoS.

#### 4.2.2 Radius for a $1.4 M_{\odot}$ star

In Fig. 7 we show contours (the U-shaped lines) of typical radius of a hybrid star, defined as  $R_{1.4}$ , the radius of a star of mass  $1.4 M_{\odot}$ , as a function of the CSS parameters. The contours only fill the part of the CSS parameter space where there are hybrid stars with that mass. The dashed (magenta) lines delimit that region which extends only up to moderate transition pressure.

The overall behavior is that, at fixed  $\Delta\epsilon/\epsilon_{\text{trans}}$ , the typical radius is large when the transition density is at its lowest. As the transition density rises the radius of a  $1.4 M_{\odot}$  star decreases at first, but then increases again. This is related to the previously noted fact [30] that when one fixes the speed of

sound of quark matter and increases the bag constant (which increases  $p_{\text{trans}}/\epsilon_{\text{trans}}$  and also varies  $\Delta\epsilon/\epsilon_{\text{trans}}$  in a correlated way) the resultant family of mass-radius curves all pass through the same small region in the  $M$ - $R$  plane: the  $M(R)$  curves “rotate” counter-clockwise around this hub (see Fig. 2 of Ref. [30]). In our case we are varying  $p_{\text{trans}}/\epsilon_{\text{trans}}$  at fixed  $\Delta\epsilon/\epsilon_{\text{trans}}$ , so the hub itself also moves. At low transition density the hub is below  $1.4 M_{\odot}$ , so  $R_{1.4}$  decreases with  $p_{\text{trans}}/\epsilon_{\text{trans}}$ . At high transition density the hub is at a mass above  $1.4 M_{\odot}$  so  $R_{1.4}$  will increase with  $p_{\text{trans}}/\epsilon_{\text{trans}}$ .

The smallest stars occur for  $c_{\text{QM}}^2 = 1$  (right hand plots), where  $R_{1.4} \gtrsim 9.5$  km at large values of the energy density discontinuity, and the radius rises as the discontinuity is decreased. This is consistent with the absolute lower bound of about 8.5 km [31] for the maximally compact  $c_{\text{QM}}^2 = 1$  star obeying  $M_{\text{max}} > 2 M_{\odot}$ .



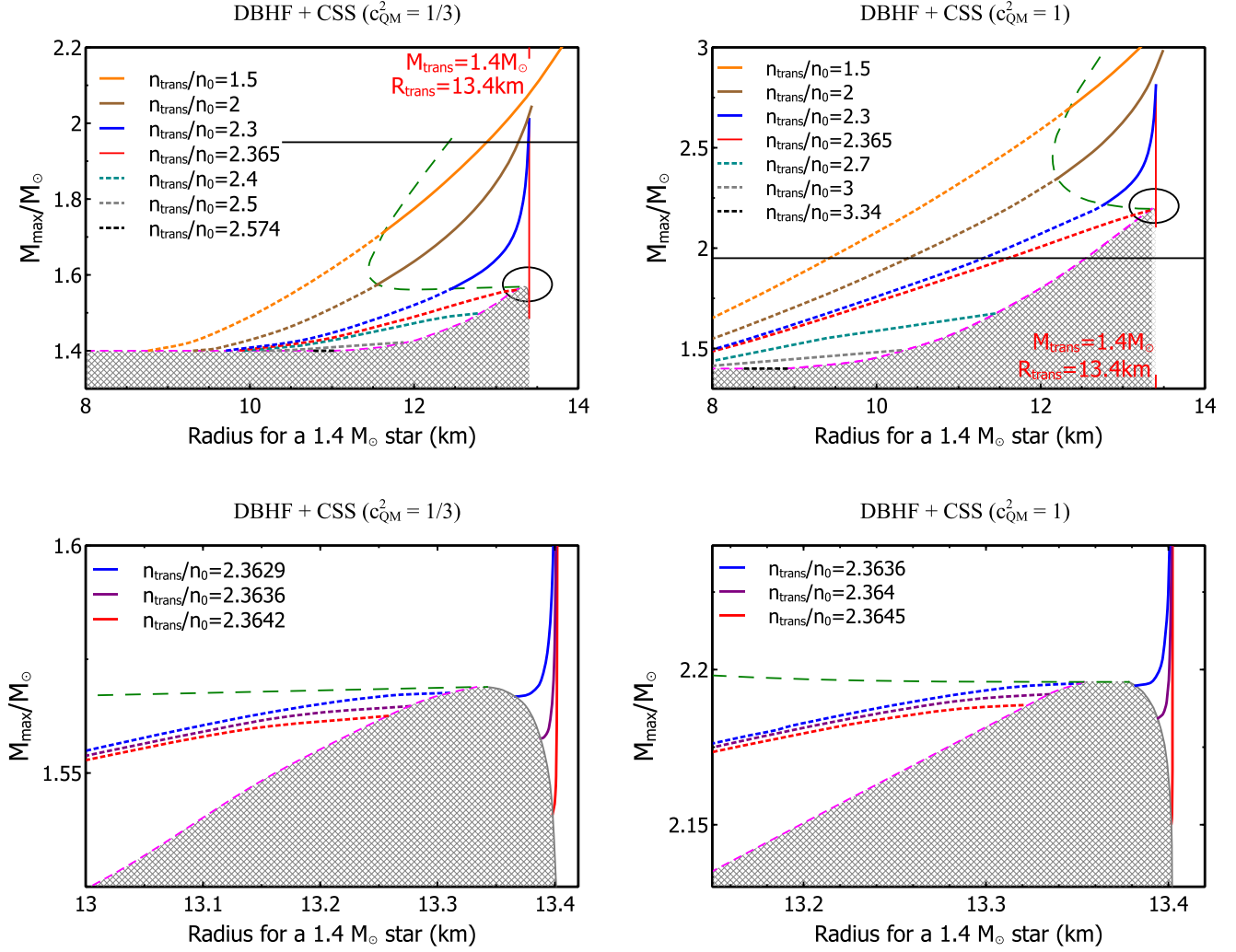


**Fig. 9.** (Color online) Contour plots showing how the maximum hybrid star mass and the radius for a  $1.4 M_{\odot}$  star vary when two of the CSS parameters, the transition density and energy density discontinuity, are varied. Shaded regions indicate where no  $1.4 M_{\odot}$  hybrid star exists. In the upper panels, EoSes below the horizontal lines (i.e. those with  $M_{\max} < 1.95 M_{\odot}$ ) are ruled out by observation, and the vertical (red) lines mark the radius for a  $1.4 M_{\odot}$  purely-hadronic star. Lower panels are zoomed in on the encircled region in the upper panels, where EoSes can give a  $1.4 M_{\odot}$  hybrid star on both connected branch (solid curves on the right) and disconnected branch (dashed curves on the left).

For  $c_{QM}^2 = 1/3$  the allowed region at low transition pressure is small, so in the right panels of Fig. 8 we show a magnification of this region. We see that in the allowed ( $M_{\max} > 1.95 M_{\odot}$  and  $n_{\text{trans}} > n_0$ ) region there is a minimum radius 12 km for the BHF (soft) hadronic EoS, and about 12.25 km for the DBHF (stiff) hadronic EoS. This minimum is attained at the lowest possible transition density,  $n_{\text{trans}} \approx n_0$ . As the transition density rises to values around  $2n_0$ , the minimum radius rises to 12.4 km (BHF) or 13.3 km (DBHF). This is comparable to the minimum radius of about 13 km found in Ref. [17], which explored a wider range of hadronic EoSes but assumed  $n_{\text{trans}} = 2n_0$ . These results are consistent with the lower bound on  $R_{1.4}$  for  $c_{QM}^2 = 1/3$  of about 11 km established in Ref. [31] (Fig. 5) using the EoS that yields maximally compact stars (corresponding to CSS with  $p_{\text{trans}} = 0$  and  $c_{QM}^2 = 1/3$ ) obeying  $M_{\max} > 2 M_{\odot}$ . If a  $1.4 M_{\odot}$  star were observed to have radius below the minimum value, one would have to conclude that it could only arise from

a CSS-type EoS if that EoS had  $c_{QM}^2 > 1/3$ . The dashed line shows how the excluded region would grow if a star of mass  $2.1 M_{\odot}$  were to be observed. This would increase the minimum radius to about 12.7 km (BHF) or 13 km (DBHF).

#### 4.3 Maximum mass vs. typical radius

Following Ref. [32], in Fig. 9 we characterize each CSS EoS by the maximum mass  $M_{\max}$  and the radius  $R_{1.4}$  of a  $1.4 M_{\odot}$  star on its mass-radius relation. We can then see which areas of the  $R_{1.4}$ - $M_{\max}$  plane can be populated by hybrid stars arising from typical nuclear EoS combined with the CSS family of quark matter EoS. Along each curve the transition density is fixed and we vary  $\Delta\epsilon/\epsilon_{\text{trans}}$ .

Each of the monotonic curves in Fig. 9 represents a family of CSS EoSes with fixed transition density, and varying

$\Delta\epsilon/\epsilon_{\text{trans}}$ . As we increase  $\Delta\epsilon/\epsilon_{\text{trans}}$ , the maximum mass on a connected branch (solid curve) decreases until it smoothly becomes the maximum mass on a disconnected branch (dashed curve) at the long-dashed (green) line, which corresponds to the nearly-horizontal phase boundary between region B and region C in the phase diagram Fig. 3. For higher transition densities the whole curve is dashed, because in that case any mass-radius curve that includes a  $1.4M_{\odot}$  hybrid star will always have its heaviest star on the disconnected branch.

The thin vertical (red) line is where the transition pressure has risen so high that it is equal to the central pressure of a nuclear matter star with a mass of  $1.4M_{\odot}$  (at  $n_{\text{trans}} = 2.365n_0$ ). Note that at higher transition pressures, although on the connected branch hybrid stars are always above  $1.4M_{\odot}$ , a  $1.4M_{\odot}$  hybrid star on the disconnected branch can still exist (see contours in upper panels of Fig. 9, where the whole curve is dashed for  $n_{\text{trans}} > 2.365n_0$ ).

On the lower panels we show contours for EoSes that can give hybrid stars on both connected branch (solid curves on the right) and disconnected branch (dashed curves on the left), at transition densities very close to but below the central density of a nuclear matter star with a mass of  $1.4M_{\odot}$  ( $n_{\text{trans}} < 2.365n_0$ ). From these plots we can see that with the same maximum mass, radii for  $1.4M_{\odot}$  hybrid stars on connected/disconnected branches can differ by from 0.1 to 0.4km.

Each plot in Fig. 9 contains a black horizontal line at  $M_{\text{max}} = 1.95M_{\odot}$ , so all EoSes that lie below that line are observationally ruled out. If  $c_{\text{QM}}^2 \lesssim 1/3$  (see left plots), the range of radii for  $1.4M_{\odot}$  hybrid stars is limited to the vicinity of the purely-hadronic star with mass  $1.4M_{\odot}$ . This is another way of illustrating the lower limit  $R > 12.25\text{km}$  found in Sec. 4.2.2 for the DBHF nuclear EoS. If  $c_{\text{QM}}^2 = 1$  (right hand plots) the range of possible radii is somewhat bigger,  $R > 9.5\text{km}$ , compatible with the radius value tracking along the  $M_{\text{max}} = 1.95M_{\odot}$  boundary in Fig. 7, upper-right panel.

## 5 Phase conversion dissipation in multicomponent compact stars

As noted in Sec. 1, it is very important to understand the dissipation mechanisms that suppress oscillations in neutron stars. One example is the damping of r-modes, which controls the spin down of neutron stars. Observational data indicates that the conventional damping mechanisms (bulk and shear viscosity) are insufficient to explain the existence of millisecond pulsars with the observed temperatures [33, 34].

Here we describe a dissipation mechanism that could account for the observations by saturating the growth of r-modes at a very low amplitude [35]. The mechanism is based on the movement of the core-mantle interface of a hybrid star in response to the pressure oscillations in the star. This requires conversion of hadronic matter into quark matter and vice versa. If the finite rate of this conversion produces a phase lag between the pressure oscillation and the position of the interface, energy will be dissipated in each cycle. We study the resultant damping and we find that this mechanism is powerful enough to saturate the r-mode at very low saturation amplitude, of order  $10^{-10}$ , and is therefore likely to be the dominant r-mode saturation mechanism in hybrid stars with a sharp interface.

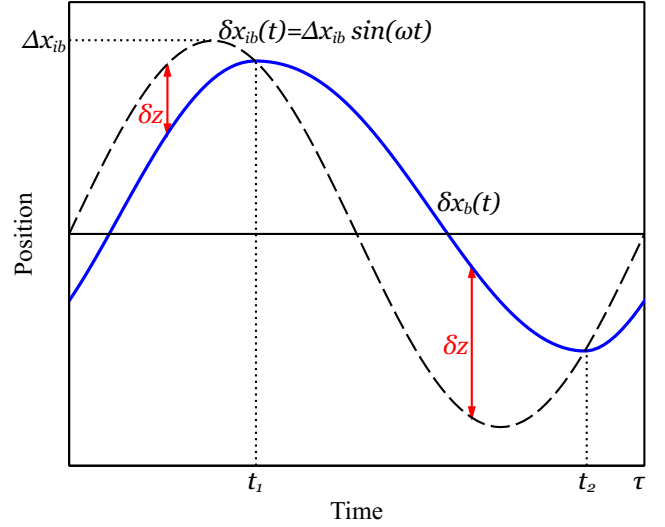


**Fig. 10.** (Color online) Diagram showing how the ideal boundary position (dashed line) and the real boundary position (solid blue line) vary in time. The ideal boundary is where the phase boundary would be if the phase conversion process equilibrated instantaneously, and it is determined by the instantaneous external pressure. The real boundary is always “chasing” the ideal boundary, with velocity given by Eq. (4) and (6) where  $\delta z(t)$  is its distance from the ideal boundary. The real boundary coincides with the ideal boundary twice per cycle, at  $t = t_1$  and  $t = t_2$ .

### 5.1 Hadron-quark conversion in a hybrid star

In a one-dimensional, simplified model describing two phases in a cylinder separated by a sharp boundary moving in response to external oscillation in the context of Newtonian gravity, the expression of the corresponding energy dissipation in one cycle of oscillation as a function of the boundary velocity is given as [35]

$$W = S \left( \frac{n_{\text{H}}}{n_{\text{L}}} - 1 \right) \left( \int_0^{\tau} \bar{p} \frac{d\delta x_b(t)}{dt} dt + \int_0^{\tau} \Delta p_{\text{L}} \sin(\omega t) \frac{d\delta x_b(t)}{dt} dt \right). \quad (3)$$

assuming that the pressure in the low-density phase oscillates harmonically with amplitude  $\Delta p_{\text{L}}$  and frequency  $\omega$  around its equilibrium value  $\bar{p}$ , and  $\bar{x}_b$  is the equilibrium position of the boundary (the center of the star is at  $x = 0$ ). Here we look at the case where the phases are quark matter and hadronic matter and are interested in situations where phase conversion dissipation becomes important in r-mode oscillations when their amplitude is still fairly low, assuming  $\delta p \ll \bar{p}$  in the region near the boundary. Therefore, we only need the EoS in a narrow pressure range around the critical pressure.

We use the calculational techniques developed by Olinto [36] to study the movement of the phase boundary in the strange matter hypothesis scenario, but we are interested in conversion of quark matter to nuclear matter as well as nuclear matter to quark matter, since both processes occur as our burning front moves inwards and outwards periodically in response to an oscillation in the pressure. The velocity of the boundary in the

NM  $\rightarrow$  QM half cycle ( $t < t_1$  and  $t > t_2$  in Fig. 10) is determined by [35]

$$\frac{d\delta x_b}{dt} \simeq \frac{1}{a_N} \sqrt{\frac{D_Q}{2\tau_Q}} \sqrt{[\delta z/\ell_Q]^2 + 2\eta_Q \delta z/\ell_Q}, \quad (4)$$

where  $\delta z \equiv |\delta x_{ib} - \delta x_b|$  is how far the boundary is from its equilibrium position at the current pressure (see Fig. 10), and  $\ell_Q$  characterizes its typical length

$$\ell_Q = \frac{(n_Q/\chi_K^Q)n_Q}{2(\gamma-1)g_b\epsilon_{\text{crit}}^N}. \quad (5)$$

In Eq. (4),  $a_N$  characterizes the strangeness fraction,  $D_Q$  is the diffusion constant for flavor,  $\tau_Q$  is the time scale of nonleptonic flavor-changing interactions,  $\eta_Q$  gives the ratio of subthermal to suprathreshold rates; in Eq. (5),  $n_Q$  is the baryon number density in equilibrated strange quark matter,  $\chi_K^Q \equiv \partial n_K/\partial \mu_K$  is the susceptibility with respect to K-ness evaluated at equilibrium,  $\gamma \equiv n_Q/n_N$  where  $n_N$  is the baryon number density in nuclear matter,  $g_b$  is the effective gravitational acceleration and  $\epsilon_{\text{crit}}^N$  is the energy density at the phase boundary on nuclear matter side (see Sec IV in [35] for detailed discussions).

The boundary velocity in the QM  $\rightarrow$  NM half cycle ( $t_1 < t < t_2$  in Fig. 10) is

$$\frac{d\delta x_b}{dt} \simeq \frac{1}{b_Q} \sqrt{\frac{D_N}{2\tau_N}} \sqrt{[\delta z/\ell_N]^2 + 2\eta_N \delta z/\ell_N} \quad (6)$$

where  $\delta z \equiv |\delta x_b - \delta x_{ib}|$  is how far the boundary is from its equilibrium position at the current pressure, with the typical length

$$\ell_N = \frac{(n_N/\chi_K^N)n_Q}{2(\gamma-1)g_b\epsilon_{\text{crit}}^N}. \quad (7)$$

and all physical quantities are defined similar to those in the NM  $\rightarrow$  QM half cycle.

Therefore with the periodic condition  $\delta x_b(t) = \delta x_b(2\pi/\omega + t)$ , Eqs. (4) and (6) fully specify the movement of the phase boundary in response to the external pressure oscillation. Next we compute the energy dissipation in this process and see whether it is capable of saturating the r-mode.

## 5.2 R-mode damping and saturation amplitude

During one cycle of an r-mode of amplitude  $\alpha$  the energy dissipated in a radially oriented cylinder with an infinitesimal base area  $dS$  straddling the phase boundary at  $(\bar{R}_b, \theta, \phi)$  is

$$dW(\alpha, \theta, \phi) = dS(\gamma-1)\Delta p_N \int_0^\tau \cos(2\phi + \omega t) \frac{d\delta R_b}{dt} dt, \quad (8)$$

where the position of the phase boundary  $\delta R_b(t)$  is assumed to move at its maximal speed [see Eqs. (4) and (6)],  $dS = \bar{R}_b^2 \sin\theta d\theta d\phi$  and the pressure oscillation is

$$\Delta p_N = g_b \epsilon_{\text{crit}}^N |\delta R_{ib}| = \epsilon_{\text{crit}}^N C_b \alpha |\sin^2\theta \cos\theta| \quad (9)$$

with  $C_b = \sqrt{\frac{105}{756\pi}} \Omega^2 \bar{R}_b^3 / R$  where  $\Omega$  and  $R$  are the rotation frequency and radius of the star.

Integrating Eq. (8) over the full range of solid angle gives the total dissipation of the r-mode in one cycle of oscillation and hence the total power dissipated,  $P_{\text{dis}}$ . The r-mode amplitude stops growing (saturates) when this equals the power injected via back-reaction from gravitational radiation  $P_{\text{gr}}$ .

As an illustrative example, Fig. 11 shows the dissipated power as a function of r-mode amplitude for a hybrid star rotating with frequency  $f = 600$  Hz, with quark core size  $\bar{R}_b/R = 0.56$  and temperature  $T = 10^8$  K. For the quark matter EoS we use the CSS parametrization introduced in Sec. 2, with  $n_{\text{trans}} = 4n_0$ ,  $\Delta\epsilon/\epsilon_{\text{trans}} = 0.2$ , and  $c_{\text{QM}}^2 = 1$ . The hadronic matter EoS is taken from Ref. [37].

In the subthermal regime, the dissipated power first rises with the r-mode amplitude  $\alpha$  as  $\alpha^3$  at very low amplitude, before entering a resonant region with a maximum in  $P_{\text{dis}}/\alpha^2$ . At high amplitude in the suprathreshold regime, the dissipated power is proportional to  $\alpha^2$ . The power in gravitational radiation from the r-mode  $P_{\text{gr}}$  rises as  $\alpha^2$ , and is also shown in Fig. 11 for this particular hybrid star. At low amplitude, the phase conversion dissipation is suppressed relative to the gravitational radiation and therefore plays no role in damping the r-mode. If other damping mechanisms are too weak to suppress the r-mode, its amplitude will grow. However, as the amplitude grows, the phase conversion dissipation becomes stronger, and in this example there is a saturation amplitude  $\alpha_{\text{sat}}$  at which it equals the gravitational radiation, and the mode stops growing.

Varying parameters such as the size of the quark matter core, rotation frequency, or temperature of the star will shift the curves in Fig. 11, and if the phase conversion dissipation is too weak then there will be no intersection point ( $P_{\text{gr}}$  will be greater than  $P_{\text{dis}}$  at all  $\alpha$ ) and phase conversion dissipation will not stop the growth of the mode. However, we can see from Fig. 11 that if saturation occurs, the resultant  $\alpha_{\text{sat}}$  is in the low-amplitude regime, where an analytical approach is available, and the saturation amplitude is extraordinarily low, of order  $10^{-12}$ . This is typical of all model hybrid stars that we investigated. We derived the analytical expression for the dissipated power in the low-amplitude regime (dashed [black] line in Fig. 11), obtaining

$$P_{\text{dis}}^{\text{sub}}(\alpha) \approx \frac{\alpha^3}{15} \left( \frac{105}{756\pi} \right)^{3/2} \frac{\gamma-1}{\Delta \tilde{p}_N} \frac{(\epsilon_{\text{crit}}^N)^2 \Omega^7 \bar{R}_b^{11}}{g_b R^3}. \quad (10)$$

where

$$\Delta \tilde{p}_N \equiv \frac{9}{b_Q^2} (\gamma-1) \frac{D_N}{\tau_N} \frac{\eta_N}{n_Q} \frac{(g_b \epsilon_{\text{crit}}^N)^2}{(n_N/\chi_K^N)} \frac{1}{\Omega^2}. \quad (11)$$

For the class of models we have analyzed, in general because in nuclear matter diffusion is less efficient ( $D_N/D_Q \approx O(10^{-2})$ ) and weak interactions take more time to proceed ( $\tau_N/\tau_Q \approx O(10^2)$ ), therefore the QM  $\rightarrow$  NM transition half cycle dominates the dissipation.

Eq. (10) allows us to assess how the strength of phase conversion dissipation depends on the various parameters involved. It is particularly sensitive to the size of the quark core, and this will be important when considering a whole family of hybrid stars with different central pressures and hence different core sizes.

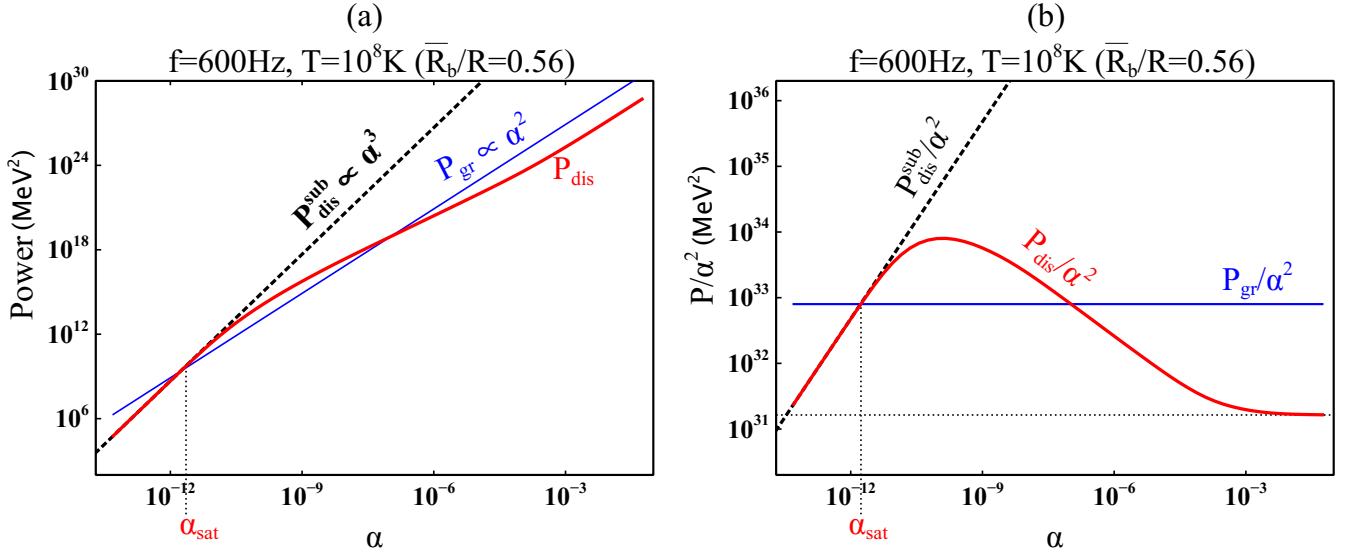


**Fig. 11.** (Color online) (a) Dissipated power due to phase conversion  $P_{\text{dis}}$  (thick solid red curve) as a function of r-mode amplitude  $\alpha$  for a specific example hybrid star (see text). (b) The same quantity where the vertical axis now shows the ratio  $P_{\text{dis}}/\alpha^2$ . At first  $P_{\text{dis}}$  is proportional to  $\alpha^3$  at very low amplitude (dashed line), then at some intermediate amplitude varies less quickly, with a maximum in  $P_{\text{dis}}/\alpha^2$ , and finally changes to  $\alpha^2$  at higher amplitude. Also shown is gravitational radiation power  $P_{\text{gr}}$  (thin solid blue straight line), which is proportional to  $\alpha^2$  at all amplitudes. The r-mode amplitude will stop growing when dissipation balances radiation, at the first point of intersection between the two curves. This defines the saturation amplitude  $\alpha_{\text{sat}}$ .

The results of such an investigation are shown in Fig. 12, where the solid (red) curve gives the numerically calculated saturation amplitude ( $\alpha_{\text{sat}}$  in Fig. 11) as a function of the size of the quark matter core in units of the star radius,  $\bar{R}_b/R$ . To construct this curve we used the hadronic and quark matter EoSes of Fig. 11 and varied the central pressure, yielding a family of different star configurations. As  $\bar{R}_b/R$  decreases, the dissipation power  $P_{\text{dis}}$  decreases rapidly relative to the gravitational radiation  $P_{\text{gr}}$ . The relative shift in the two corresponding curves in Fig. 11 leads to an upper limit on  $\alpha_{\text{sat}}$  when  $P_{\text{gr}}$  is tangent to  $P_{\text{dis}}$ . This corresponds to the end of the solid curve in Fig. 12 at  $\alpha_{\text{sat}}^{\text{max}}$  at the critical value of the quark core size,  $(\bar{R}_b/R)_{\text{crit}}$ , below which the phase-conversion mechanism cannot saturate the r-mode any more.

The black dashed curve in Fig. 12 is the low-amplitude analytical approximation to  $\alpha_{\text{sat}}$

$$\begin{aligned} \alpha_{\text{sat}}^{\text{approx}} &= \left( \frac{2^{22} \pi^{9/2}}{3^3 \cdot 5^{5/2}} \right) G \frac{\bar{D}_N}{\tau_N} \frac{(\chi_K^N)^3}{n_Q n_N^3 b_Q^2} \frac{g_b^3 M^2 \bar{f}^2}{\Omega} \frac{R^9}{\bar{R}_b^{11}} \\ &\approx 4.2 \times 10^{-11} \gamma \left( \frac{\bar{D}_N}{1.5 \text{ MeV}^3} \right) \left( \frac{\tau_N}{2 \times 10^{-8} \text{ s}} \right)^{-1} \\ &\times \left( \frac{b_Q}{1/3} \right)^{-2} \left( \frac{n_N}{2n_0} \right)^{-4} \left( \frac{\chi_K^N}{(100 \text{ MeV})^2} \right)^3 \left( \frac{g_b}{g_u} \right)^3 \\ &\times \left( \frac{\epsilon_{\text{crit}}^Q}{2 \epsilon_{\text{crit}}^N} \right)^3 \left( \frac{\epsilon_{\text{crit}}^N}{600 \text{ MeV fm}^{-3}} \right)^3 \left( \frac{M}{1.4 M_\odot} \right)^2 \\ &\times \left( \frac{\bar{f}}{0.02} \right)^2 \left( \frac{f}{1 \text{ kHz}} \right)^{-1} \left( \frac{R}{10 \text{ km}} \right) \left( \frac{\bar{R}_b/R}{0.4} \right)^{-8}, \quad (12) \end{aligned}$$

where  $D_N \equiv \bar{D}_N \times T^{-2}$ , and  $g_u$  is the Newtonian gravitational acceleration at the phase boundary when the quark core has uniform density  $\epsilon = \epsilon_{\text{crit}}^Q$  ( $g_u \equiv \frac{4}{3} \pi G \epsilon_{\text{crit}}^Q \bar{R}_b$ ). This approximation is very accurate when the phase conversion damping is strong, but it does not capture the sudden weakening of that dissipation when, for example, the core radius becomes small.

### 5.3 Range of validity of low-amplitude approximation

The range of validity of Eqs. (10) and (12) is found by calculating the next-to-leading (NLO) contribution, and requiring that it be less than a fraction  $\epsilon$  of the total dissipated power. We find that the approximation is valid when

$$\begin{aligned} \epsilon &\geq \frac{2^{39} \pi^5}{3^{12} 5^4} \frac{G^2}{(\gamma-1)^2} \frac{g_b M^4 \bar{f}^4 \Omega^6}{(\epsilon_{\text{crit}}^N)^2} \left( \frac{R}{\bar{R}_b} \right)^{16} \\ &\simeq 2.96 \left( \frac{\gamma-1}{0.5} \right)^{-2} \left( \frac{\epsilon_{\text{crit}}^Q}{2 \epsilon_{\text{crit}}^N} \right)^2 \left( \frac{g_b}{g_u} \right)^2 \left( \frac{M}{1.4 M_\odot} \right)^4 \\ &\times \left( \frac{\bar{f}}{0.02} \right)^4 \left( \frac{f}{1 \text{ kHz}} \right)^6 \left( \frac{R}{10 \text{ km}} \right)^2 \left( \frac{\bar{R}_b/R}{0.4} \right)^{-14}. \quad (13) \end{aligned}$$

We see that the validity of the low-amplitude approximation is mainly determined by the size of the quark matter core and the rotation frequency of the star.

### 5.4 Discussion

We have described how phase conversion in a multicomponent compact star provides a mechanism for damping density oscillations.

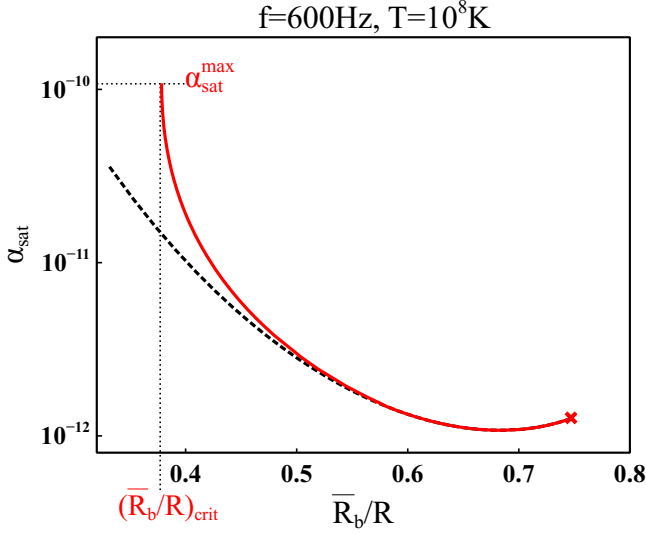


**Fig. 12.** (Color online) R-mode saturation amplitude (red solid curve) and its low-amplitude analytical approximation (black dashed curve) as a function of the radius of the quark matter core  $\bar{R}_b$  divided by the star radius  $R$  in a family of hybrid stars. For  $\bar{R}_b/R < (\bar{R}_b/R)_{\text{crit}} \approx 0.38$ , damping is too weak to saturate the r-mode. At  $\bar{R}_b/R \gtrsim 0.75$  the hybrid star is unstable against gravitational collapse. The mass fraction of the core is in the range  $0.12 \lesssim M_{\text{core}}/M_{\text{star}} \lesssim 0.68$  for all the configurations shown on the red solid curve.

lations, via the phase lag in the response of the interface between components of different baryon densities to the applied pressure oscillation. The phase lag arises from the finite rate of interconversion between the phases, which limits the speed with which the interface can move. We studied the case where the two phases are separated by a sharp boundary (first-order phase transition) and analyzed the movement of the interface in the approximation of a steady state, neglecting additional acceleration effects and complicated hydrodynamic effects like turbulence. In particular, we studied the astrophysically interesting case of the damping of r-mode oscillations [6, 7] in a two-component star. We found that phase conversion dissipation does not affect the r-mode instability region, because it vanishes as  $\alpha^3$  at low r-mode amplitude  $\alpha$ . However, depending on the values of relevant parameters, phase conversion dissipation can either saturate the r-mode at extremely low amplitudes,  $\alpha_{\text{sat}} \lesssim 10^{-10}$  in the explicit example of hadron-quark transformation at the sharp quark-hadron interface in a hybrid star, or be insufficient to saturate the r-mode at all. The reason for this behavior stems, analogously to the bulk viscosity [38], from the resonant character of the dissipation, which is relatively strong when the time scale of the dissipation matches the time scale of the external oscillation (see Fig. 11). Whether saturation is possible depends therefore on the microscopic and astrophysical parameters, like in particular on the mass of the quark core, which should not be too small.

Our main result is Eq. (8), which must be evaluated using numerical solutions of Eqs. (4) and (6). We also give the low-amplitude analytic expressions for the power dissipated [Eq. (10)] and the saturation amplitude [Eq. (12)] which are

valid when the dissipation is sufficiently strong, obeying Eq. (13) with  $\varepsilon \ll 1$ .

Our results have significant implications for astrophysical signatures of exotic high-density phases of matter, such as quark matter. The observed data for millisecond pulsars is not consistent with the minimal model of pulsars as stars made of nuclear matter with damping of r-modes via bulk and shear viscosity [34]. Resolving this discrepancy requires either a new mechanism for stabilizing r-modes, or a new mechanism for saturating unstable r-modes at  $\alpha_{\text{sat}} \lesssim 10^{-8} - 10^{-7}$  [39, 34, 40]. Previously proposed mechanisms have problems to achieve this. Suprathreshold bulk viscosity and hydrodynamic oscillations both give  $\alpha_{\text{sat}} \sim 1$  [41, 42]. The nonlinear coupling of the r-mode to viscously damped daughter modes could give  $\alpha_{\text{sat}} \sim 10^{-6}$  to  $10^{-3}$  [43, 44]. The recently proposed vortex-fluxtube cutting mechanism [45] might give sufficiently small saturation amplitudes but is present only at sufficiently low temperatures  $T \ll T_c \lesssim 10^9$  K, which could be exceeded by the r-mode (and/or accretion) heating [34]. One of the main results of this paper is that phase conversion dissipation can provide saturation at the required amplitude to explain millisecond pulsar data.

Second, due to the extremely low r-mode saturation amplitude of our proposed mechanism, hybrid stars would behave very differently from neutron or strange stars. As discussed in Ref. [34], if the known millisecond sources were hybrid stars then, for the low saturation amplitudes that we have found, they would have cooled out of the r-mode instability region quickly (in millions of years) so that they would have very low temperatures by now. In contrast, in neutron stars r-modes would be present and would provide such strong heating that the temperature of observed millisecond pulsars would be  $T_{\infty} \sim O(10^5 - 10^6)$  K [34]. This prediction assumes a (so far unknown) saturation mechanism that would saturate the mode at a value  $\alpha_{\text{sat}} \lesssim 10^{-8}$  required by the pulsar data. This temperature is significantly higher than what standard cooling estimates suggest for such old sources. The same holds for strange quark stars where the enhanced viscous damping can explain the pulsar data, but even in this case the star would spin down along the boundary of the corresponding stability window which would keep it at similarly high temperatures. Measurements of or bounds on temperatures of isolated millisecond pulsars provide therefore a promising way to discriminate hybrid stars.

## 6 Summary and outlook

In this paper we studied how strange quark matter could influence the static properties and dynamic behaviors of hybrid stars in two ways.

Firstly we explored the CSS (Constant Speed of Sound) parameterization of the quark matter EoS, which assumes a sharp transition from nuclear matter to quark matter, and that the speed of sound in quark matter is independent of the pressure. Our study is intended to motivate the use of the CSS parameterization as a framework in which the implications of observations of neutron stars for the high-density EoS can be expressed and discussed in a way that is reasonably model-independent. We showed how mass and radius observations can be expressed as constraints on the three CSS parameters, and we found that



the observation of a  $2.0M_{\odot}$  star already constrains the CSS parameters significantly.

If, as predicted by many models,  $c_{\text{QM}}^2 \lesssim 1/3$ , then there are two possible scenarios: a low-transition-pressure scenario, where the transition to the high density phase occurs at  $n_{\text{trans}} \lesssim 2n_0$ , and a high-transition-pressure scenario. In the low-transition-pressure case there are strong constraints on the radius of the star, as shown in Fig. 8. The radius of the maximum mass star (which is typically the smallest possible star) must be greater than about 11.25 km, and the radius of a  $1.4M_{\odot}$  star must be greater than about 12 km [31]. The high-transition-pressure case corresponds to the white region on the right side of the left panels of Figs. 5, 6, 7, which tends to give a very small branch of hybrid stars with tiny quark matter cores, occurring in a narrow range of central pressures just above the transition pressure.

If  $c_{\text{QM}}^2$  is larger than  $1/3$  then a larger region of the CSS parameter space becomes allowed. The right panels of Figs. 5, 6, 7 show the extreme case where  $c_{\text{QM}}^2 = 1$ . In this case the minimum possible radius is around 9.0 km, and the radius of a  $1.4M_{\odot}$  star must be greater than about 9.5 km.

In the second part of the paper we studied a dissipation mechanism that is expected to occur in hybrid stars with a sharp boundary between the quark matter and the nuclear matter. The mechanism is phase conversion dissipation, and we found that it can saturate an unstable r-mode with an amplitude in the range  $O(10^{-12})$  to  $O(10^{-10})$ . This is of the right order to explain millisecond pulsar data. We gave an analytical form of the saturation amplitude, with its dependence on a set of parameters such as quark core size, rotation frequency and so on. More measurements of temperatures would give more information about the r-mode amplitude and therefore help probe the compositions of hybrid stars.

As well as the quark-hadron interface in a hybrid star, any first-order phase transition that leads to a sharp interface between two phases with different baryon densities could lead to phase conversion dissipation of global pressure oscillation modes. For example, such dissipation could occur at the boundary between different phases of quark matter.

Our discussion was limited to the case of a sharp interface, which is the expected configuration if the surface tension is large enough. If the surface tension is small, there will instead be a mixed phase region where domains of charged hadronic and quark matter coexist. We expect that the phase conversion dissipation mechanism will operate in this case too, as the domains expand and shrink in response to pressure oscillations. A similar mechanism should also be relevant for the “nuclear pasta” mixed phases in the inner crust of an ordinary neutron star. In this case in addition to the slow beta-equilibration processes there may also be slow strong interaction equilibration processes, whose rate is suppressed by tunneling factors for the transition between geometric domains of different size. This could further enhance the dissipation.

## References

1. M. G. Alford, K. Rajagopal, S. Reddy, and F. Wilczek, *The Minimal CFL nuclear interface*, Phys.Rev. **D64** (2001) 074017, [hep-ph/0105009].
2. L. F. Palhares and E. S. Fraga, *Droplets in the cold and dense linear sigma model with quarks*, Phys.Rev. **D82** (2010) 125018, [arXiv:1006.2357].
3. M. B. Pinto, V. Koch, and J. Randrup, *The Surface Tension of Quark Matter in a Geometrical Approach*, arXiv:1207.5186.
4. J. Macher and J. Schaffner-Bielich, *Phase transitions in compact stars*, Eur.J.Phys. **26** (2005) 341–360, [astro-ph/0411295].
5. K. Masuda, T. Hatsuda, and T. Takatsuka, *Hadron-Quark Crossover and Massive Hybrid Stars*, arXiv:1212.6803.
6. N. Andersson, *A New class of unstable modes of rotating relativistic stars*, Astrophys.J. **502** (1998) 708–713, [gr-qc/9706075].
7. N. Andersson and K. D. Kokkotas, *The R mode instability in rotating neutron stars*, Int.J.Mod.Phys. **D10** (2001) 381–442, [gr-qc/0010102].
8. M. G. Alford, S. Han, and M. Prakash, *Generic conditions for stable hybrid stars*, Phys.Rev. **D88** (2013), no. 8 083013, [arXiv:1302.4732].
9. J. Zdunik and P. Haensel, *Maximum mass of neutron stars and strange neutron-star cores*, Astron. Astrophys. **551** (Mar., 2013) A61, [arXiv:1211.1231].
10. N. Chamel, A. Fantina, J. Pearson, and S. Goriely, *Maximum mass of neutron stars with exotic cores*, Astron. Astrophys. **553** (2013) A22, [arXiv:1205.0983].
11. B. Agrawal, *Equations of state and stability of color-superconducting quark matter cores in hybrid stars*, Phys.Rev. **D81** (2010) 023009, [arXiv:1001.1584].
12. L. Bonanno and A. Sedrakian, *Composition and stability of hybrid stars with hyperons and quark color-superconductivity*, Astron.Astrophys. **539** (2012) A16, [arXiv:1108.0559].
13. R. Lastowiecki, D. Blaschke, H. Grigorian, and S. Typel, *Strangeness in the cores of neutron stars*, Acta Phys.Polon.Supp. **5** (2012) 535–540, [arXiv:1112.6430].
14. A. Kurkela, P. Romatschke, A. Vuorinen, and B. Wu, *Looking inside neutron stars: Microscopic calculations confront observations*, arXiv:1006.4062.
15. M. Alford, M. Braby, M. Paris, and S. Reddy, *Hybrid stars that masquerade as neutron stars*, Astrophys.J. **629** (2005) 969–978, [nucl-th/0411016].
16. M. G. Alford, G. Burgio, S. Han, G. Taranto, and D. Zappal, *Constraining and applying a generic high-density equation of state*, arXiv:1501.0790.
17. P. F. Bedaque and A. W. Steiner, *Sound velocity bound and neutron stars*, Phys.Rev.Lett. **114** (2015) 031103, [arXiv:1408.5116].
18. T. Kojo, P. D. Powell, Y. Song, and G. Baym, *Phenomenological QCD equation of state for massive neutron stars*, Phys.Rev. **D91** (2015), no. 4 045003, [arXiv:1412.1108].
19. S. Benic, *Heavy hybrid stars from multi-quark interactions*, Eur.Phys.J. **A50** (2014) 111, [arXiv:1401.5380].
20. R. Schaeffer, L. Zdunik, and P. Haensel, *Phase transitions in stellar cores. I - Equilibrium configurations*, Astron. Astrophys. **126** (Sept., 1983) 121–145.
21. L. Lindblom, *Phase transitions and the mass radius curves of relativistic stars*, Phys.Rev. **D58** (1998) 024008, [gr-qc/9802072].
22. T. Gross-Boelting, C. Fuchs, and A. Faessler, *Covariant representations of the relativistic Bruckner T matrix and the nuclear matter problem*, Nucl.Phys. **A648** (1999) 105–137, [nucl-th/9810071].
23. G. Taranto, M. Baldo, and G. Burgio, *Selecting microscopic Equations of State*, Phys.Rev. **C87** (2013) 045803, [arXiv:1302.6882].

24. J. M. Bardeen, K. S. Thorne, and D. W. Meltzer, *A Catalogue of Methods for Studying the Normal Modes of Radial Pulsation of General-Relativistic Stellar Models*, The Astrophysical Journal **145** (Aug., 1966) 505.
25. Z. F. Seidov, *The Stability of a Star with a Phase Change in General Relativity Theory*, Sov. Astron. **15** (Oct., 1971) 347.
26. N. K. Glendenning and C. Kettner, *Possible third family of compact stars more dense than neutron stars*, Astron. Astrophys. **L9** (2000) 353.
27. K. Schertler, C. Greiner, J. Schaffner-Bielich, and T. M. H., *Quark phases in neutron stars and a "third family" of compact stars as a signature for phase transitions*, Nucl. Phys. **A677** (2000) 463, [astro-ph/0001467].
28. J. Antoniadis, P. Freire, N. Wex, T. Tauris, R. Lynch, and et al., *A Massive Pulsar in a Compact Relativistic Binary*, Science **340** (2013) 1233232, [arXiv:1304.6875].
29. P. Demorest, T. Pennucci, S. Ransom, M. Roberts, and J. Hessels, *Shapiro Delay Measurement of A Two Solar Mass Neutron Star*, Nature **467** (2010) 1081–1083, [arXiv:1010.5788].
30. A. V. Yudin, T. L. Razinkova, D. K. Nadyozhin, and A. D. Dolgov, *Special point on the mass-radius diagram of hybrid stars*, Astronomy Letters **40** (apr, 2014) 201–211, [arXiv:1404.0865].
31. J. M. Lattimer, *The nuclear equation of state and neutron star masses*, Ann.Rev.Nucl.Part.Sci. **62** (2012) 485–515, [arXiv:1305.3510].
32. J. M. Lattimer, "Neutron stars and core-collapse supernovae." APS 2015 April Meeting.  
<http://meetings.aps.org/link/BAPS.2015.APR.R9.1>.
33. W. C. G. Ho, N. Andersson, and B. Haskell, *Revealing the Physics of r Modes in Low-Mass X-Ray Binaries*, Physical Review Letters **107** (Sept., 2011) 101101, [arXiv:1107.5064].
34. M. G. Alford and K. Schwenzer, *What the Timing of Millisecond Pulsars Can Teach us about Their Interior*, Phys.Rev.Lett. **113** (2014) 251102, [arXiv:1310.3524].
35. M. G. Alford, S. Han, and K. Schwenzer, *Phase conversion dissipation in multicomponent compact stars*, Phys.Rev. **C91** (2015), no. 5 055804, [arXiv:1404.5279].
36. A. V. Olinto, *On the Conversion of Neutron Stars Into Strange Stars*, Phys.Lett. **B192** (1987) 71.
37. K. Hebeler, J. Lattimer, C. Pethick, and A. Schwenk, *Constraints on neutron star radii based on chiral effective field theory interactions*, Phys.Rev.Lett. **105** (2010) 161102, [arXiv:1007.1746].
38. M. G. Alford, S. Mahmoodifar, and K. Schwenzer, *Large amplitude behavior of the bulk viscosity of dense matter*, J.Phys. **G37** (2010) 125202, [arXiv:1005.3769].
39. S. Mahmoodifar and T. Strohmayer, *Upper Bounds on r-mode Amplitudes from Observations of Low-mass X-Ray Binary Neutron Stars*, Astrophys.J. **773** (2013) 140, [arXiv:1302.1204].
40. B. Haskell, N. Degenaar, and W. C. Ho, *Constraining the physics of the r-mode instability in neutron stars with X-ray and UV observations*, Mon.Not.Roy.Astron.Soc. **424** (2012) 93, [arXiv:1201.2101].
41. M. G. Alford, S. Mahmoodifar, and K. Schwenzer, *Viscous damping of r-modes: Large amplitude saturation*, Phys.Rev. **D85** (2012) 044051, [arXiv:1103.3521].
42. L. Lindblom, J. E. Tohline, and M. Vallisneri, *Nonlinear evolution of the r modes in neutron stars*, Phys.Rev.Lett. **86** (2001) 1152–1155, [astro-ph/0010653].
43. J. Brink, S. A. Teukolsky, and I. Wasserman, *Nonlinear couplings of R-modes: Energy transfer and saturation amplitudes at realistic timescales*, Phys.Rev. **D70** (2004) 121501, [gr-qc/0406085].
44. R. Bondarescu and I. Wasserman, *Nonlinear Development of the R-Mode Instability and the Maximum Rotation Rate of Neutron Stars*, Astrophys.J. **778** (2013) 9, [arXiv:1305.2335].
45. B. Haskell, K. Glampedakis, and N. Andersson, *A new mechanism for saturating unstable r-modes in neutron stars*, Mon.Not.Roy.Astron.Soc. **441** (2014) 1662, [arXiv:1307.0985].